ACS Photonics

Article

pubs.acs.org/journal/apchd5

Transparent Conductive Oxides as Near-IR Plasmonic Materials: The Case of Al-Doped ZnO Derivatives

Arrigo Calzolari,*[,†] Alice Ruini,[†,‡] and Alessandra Catellani[†,§]

[†]Istituto Nanoscienze CNR-NANO-S3, I-41125 Modena, Italy

[‡]Dipartimento di Fisica, Informatica e Matematica, Universitá di Modena e Reggio Emilia, I-41125 Modena, Italy

[§]CNR-IMEM, Parco Area delle Scienze, 37A, I-43100 Parma, Italy

Supporting Information

ABSTRACT: Using first-principles calculations, we investigate the origin of near-infrared plasmonic activity in Al:ZnO transparent conducting oxides. Our results predict realistic values for the plasma frequency and the free electron density as a function of the Al doping and in agreement with recent experimental results. We also provide a microscopic insight on the formation of surface-plasmon polaritons at the Al:ZnO/ZnO interfaces in terms of characteristic lengths that can be measured by experiments. The direct comparison with standard plasmonic metals underlines the promising capabilities of transparent conducting oxides as compact and low-loss plasmonic materials for optoelectronic applications and telecommunications.

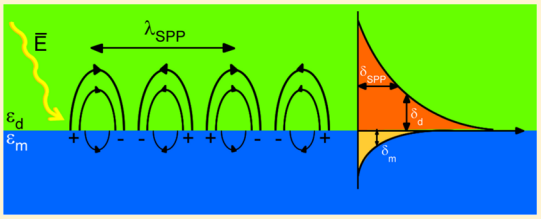

KEYWORDS: *TCO, plasmonics, surface-plasmon polariton, Al-doped ZnO, DFT*

Plasmonics has gained a paramount interest in the scientific community in view of the possibility of amplifying and confining electromagnetic fields to regions below the diffraction limits.[1,2] This allows one to conjugate the compactness of electronic devices and the speed of photonic systems, opening up a wide range of applications as metamaterials,[3−5] optical antennas,[6−9] sensors, and waveguides[10,11] that can be exploited for photoenergy conversions,[12−16] biomedical diagnostics,[17−20] light-emitters,[16,21−24] and telecommunications.[25,26] All of those applications rely on the possibility of exciting plasmons, i.e., collective oscillations of free charges, in metal nanoparticles (localized surface plasmons) or at dielectric/metal interfaces (surface-plasmon polaritons, SPPs), as a response to an applied electric field. In both cases, the prerequisites for having good plasmonic materials are (1) abundance of free electron charge and (2) low energy loss, which means, in terms of the dielectric function $\hat{\epsilon} = \epsilon' + i\epsilon''$ of the material, that (1) $\epsilon' < 0$ and (2) $\epsilon'' \approx 0$.[27]

Noble metals (especially Au and Ag) are typical plasmonic materials; however, they exhibit large energy losses, especially in the visible and UV spectral ranges, arising in part from interband electronic transitions and in part from dissipative events (e.g., el−el, el−ph scattering), which are detrimental to the performance of plasmonic devices. Semiconductors are conventionally regarded as dielectric materials for frequencies above several hundred THz, and they can exhibit a negative real permittivity only upon heavy doping. However, the doping dosage required to shift the plasma frequency from UV to NIR is in many cases too high to be achieved without damaging the semiconductor sample, preventing applications of standard semiconductors (e.g., Si, III-V) as plasmonic materials. A novel class of materials has been recently proposed that combine excellent dc conductivity with high optical transparency in the visible and NIR range: transparent conductive oxides (TCOs),[26,28−30] such as indium tin oxide (ITO) and metal-doped ZnO derivatives, have large bandgaps (E_g > 3 eV), optical absorption in the UV region (i.e., low energy loss), and quasi-parabolic conduction bands (i.e., highly dispersive), which allows for the formation of a free electron gas, upon doping. Finally, those oxides can sustain large metal (e.g., Al, Ga, In) doping up to 3−5%, without remarkable structural distortions.[31,32]

The success of ZnO-based TCOs for optoelectronic applications, such as solar cells and liquid crystal displays, and for plasmonic applications in the NIR-visible range is related to the high versatility of ZnO, which can be easily grown in ordered arrays of nanostructures, such as wires, that may be easily integrated in nanoscale devices,[33,34] with the further advantage of a relatively low production cost, with respect to noble metals. The evidence of bulk-like plasmon activity of metal-doped ZnO derivatives in the NIR-vis regime[25,35−37] has promptly stimulated their application for the realization of hybrid architectures with dielectric materials. Particularly interesting is the coupling of the plasmonic Al-doped ZnO and the dielectric ZnO: The combination of lattice matched interfaces and tunable operating frequencies has recently allowed the realization of superstructures with superior plasmonic properties.[37] This new class of TCO-based metamaterials opens the way for application as transformation optics and telecommunications.

Received: April 11, 2014
Published: July 3, 2014

 © 2014 American Chemical Society

It has also been demonstrated that such interfaces may promote formation and propagation of surface-plasmon polaritons (SPPs) that can well confine the electromagnetic (EM) radiation, in analogy with more standard metal/dielectric interfaces usually affected by larger losses and worse confinement in the low-energy region of the EM spectrum.[30]

While for noble metals the plasma frequency and the other plasmonic properties can be extracted once and for all from experimental data, in the case of TCOs, this is not possible because of the doping-induced modifications in the optoelectronic properties of the host material. In this paper, we present a first-principles investigation of the electronic, optical, and plasmonic properties of Al-doped ZnO (AZO), taken as prototypical TCO material, in the important and less exploited range of applications of THz. In particular, we provide a microscopic study of the effect of Al-doping concentration on the plasmon properties of realistic AZO bulk systems, and we then investigate the formation of SPPs at the AZO/ZnO interface. Our results reveal the microscopic mechanisms that regulate the plasmonic behavior in these materials, and complement the newest experimental findings[30] in confirming that ZnO TCOs are very promising materials for plasmonic applications.

THEORY AND COMPUTATIONAL DETAILS

For the description of the optical properties of bulk-like systems, we adopted a generalized Drude−Lorentz expression of the macroscopic dielectric function $\hat{\epsilon}(\omega)$,[27] evaluated via a first-principles approach, where both intraband (Drude-like) and interband (Lorentz-like) contributions are explicitly taken into account. For a small wavevector $\mathbf{q}$ of the external radiation ($\mathbf{q} \to 0$, dipole approximation), the complex dielectric function reads[38]

$$\hat{\epsilon}(\omega) = 1 - \sum_{\mathbf{k},n} f_{\mathbf{k}}^{n,n} \frac{{\omega_p}^2}{\omega^2 + i\eta\omega} + \sum_{\mathbf{k},n\neq n'} f_{\mathbf{k}}^{n,n'} \frac{{\omega_p}^2}{{\omega_{\mathbf{k},n,n'}}^2 - \omega^2 - i\Gamma\omega} \quad (1)$$

where

$$\omega_p = \sqrt{\frac{4\pi e^2 N_e}{m^*}} \quad (2)$$

is the bulk plasma frequency; $\hbar\omega_{\mathbf{k},n,n'} = E_{\mathbf{k},n} - E_{\mathbf{k},n'}$ is the vertical band-to-band transition energy between occupied and empty Bloch states, labeled by the quantum numbers $\{\mathbf{k}, n\}$ and $\{\mathbf{k}, n'\}$. η, $\Gamma \to 0^+$ are the Drude-like and Lorentz-like relaxation terms, while $f_{\mathbf{k}}^{n,m}$ and $f_{\mathbf{k}}^{n,n'}$ are the corresponding oscillator strengths that are related to the dipole matrix elements between Bloch states (see the Supporting Information for further details).

Within the random phase approximation, the crystal system can be easily described by a set of independent particle eigenfunctions ($\psi_{\mathbf{k},n} = u_{\mathbf{k},n} e^{i\mathbf{k}\cdot\mathbf{r}}$) and eigenvalues ($E_{\mathbf{k},n}$) that can be obtained by solving a Kohn−Sham density functional theory (DFT) problem. Once the DFT electronic structure for occupied and empty states is reached, Bloch functions ($\psi_{\mathbf{k},n} = u_{\mathbf{k},n} e^{i\mathbf{k}\cdot\mathbf{r}}$) and energy eigenvalues ($E_{\mathbf{k},n}$) are used to evaluate the oscillator strengths and the Lorentzian functions that enter in eq 1.

We calculated the electronic properties of ZnO and AZO bulk systems using the PBE-GGA[39] implementation of DFT, as coded in the Quantum ESPRESSO package. We used ultrasoft pseudopotentials[40] for all of the atomic species and a 28 (280) Ry energy cutoff in the plane wave expansion of wave functions (charge). 3d electrons of Zn have been explicitly included in the valence for both cases. A Hubbard-like potential with U = 12.0 eV and U = 6.5 eV is applied on the 3d orbitals of zinc and on the 2p orbitals of oxygen, respectively.[41] This is an efficient and computationally inexpensive way to correct for the severe underestimation of the bandgap and the wrong energy position of the d-bands of the Zn atoms.[42,43]

Different doped systems were investigated, as obtained by varying the number of substitutional Al atoms in the range 0−3.2%, in the virtual crystal approximation. ZnO and AZO bulks are simulated using periodically repeated orthorhombic supercells, including 64 (128) atoms for 0, 1.6, and 3.2% (0.8%) doping. We used a $6 \times 4 \times 6$ ($3 \times 4 \times 6$) k-point grid to sample the complete Brillouin zone of smaller (larger) systems. All structures were relaxed until forces on all atoms were lower than 0.03 eV/A.

The dielectric function has been calculated using the model described above and implemented in the code *epsilon.x*, also included in the QUANTUM ESPRESSO suite. Once the complete dielectric function is known, the electron energy loss function can be easily obtained as $L(\omega) = \mathrm{Im}\{-1/\hat{\epsilon}\}$.

BULK PLASMONS IN AZO CRYSTALS

Most of the TCO and plasmonic properties of AZO directly stem from the peculiar shape of the bottom of the ZnO conduction band, which is characterized by a single and almost parabolic band along the full Brilloun zone (see Figure 1). This

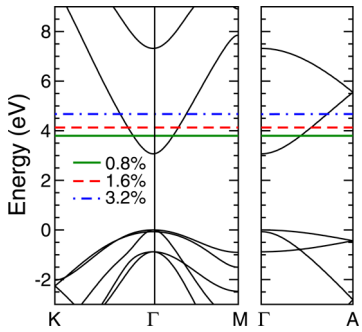

Figure 1. Fermi level (horizontal lines) alignment corresponding to different Al dosages, with respect to the ZnO bulk band structure. The zero energy reference is set to the top of the ZnO valence band.

implies a quasi-free electron gas behavior for conduction charge. The corresponding effective masses for electrons, m_e^*—evaluated as the inverse of the second derivative of the energy bands versus the crystalline momentum $\mathbf{k}$—is 0.29 m_0, in good agreement with the experimental value (0.27 m_0).[44]

Within the solubility limit (~3.5%),[31,45] Al dopants mostly assume Zn-substitutional sites, and the crystalline order of the ZnO host is only slightly perturbed. This has two main effects on the electronic structure of AZO:[31] (i) Al does not induce the formation of defect states in the ZnO bandgap, and (ii) Al donates its 3p electron to the ZnO conduction band, without remarkably changing the shape and the curvature of the conduction band minimum. Different Al dosages actually correspond to a different amount of the free charge injected

dx.doi.org/10.1021/ph500118y | ACS Photonics 2014, 1, 703−709

into the ZnO conduction band. This is described in Figure 1, where the horizontal lines identify the calculated Fermi levels of AZO at different Al amounts. This is the typical fingerprint of an intrinsic n-type conductor. In virtue of the single quasi-parabolic band[46,47] at the ZnO bottom of the conduction bands, the effect of Al doping is the formation of a free electron gas in the metal oxide. This is the fundamental prerequisite for a plasmonic material, which in the present case is realized as a trade-off between free electron charge with high mobility and relatively small electron density, if compared to noble metals.[30]

By using the Drude−Lorentz model described above, we calculated the imaginary and real parts of the dielectric function, along with the corresponding loss function. Results are summarized in Figure 2. Panel a reproduces the

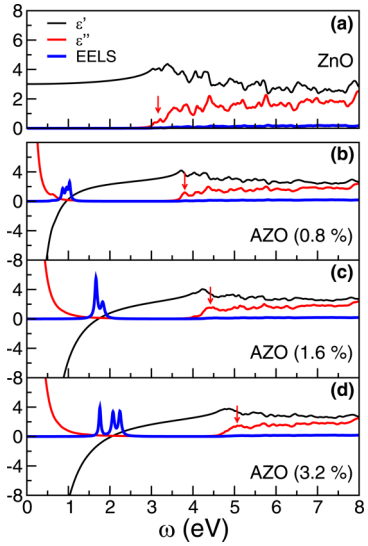

Figure 2. Real (black line) and imaginary (red line) parts of the complex dielectric function $\hat{\epsilon}$ and the electron energy loss function (blue line) of bulk ZnO (a) and AZO (b−d) at different Al concentrations. Vertical arrows mark the interband absorption edges.

characteristics of ZnO, taken as reference. The dielectric function has the behavior typical of semiconductors: in the considered energy range, ϵ' is always positive and reaches the dielectric constant value ($\epsilon^{\infty} = 3.0$) in the $\omega \rightarrow 0^{+}$ limit, in agreement with experimental spectroscopic ellipsometry data ($\epsilon^{\infty} = 3.7$)[48] and previous theoretical reports.[49,50] The lowest energy peak of ϵ'' is at 3.3 eV (vertical arrow, Figure 2), which corresponds to an interband absorption edge in the UV range. This is responsible for the transparency of the ideal ZnO material.[51]

The inclusion of Al doping changes this picture (Figure 2b−d). We distinguish two energy regions. In the UV range, the imaginary part of the dielectric function has a net peak, whose energy position depends on the doping level. This corresponds to the interband valence-to-conduction absorption edge. In all cases, there is a hypsochromic shift of the absorption edge that may be explained in terms of the Burnstein−Moss effect.[31,52] The transparency in the visible range along with the electrical n-type characteristics are unambiguously linked to the TCO properties of AZO compounds.

At lower frequencies, the optical properties of AZO completely differ from the original ZnO ones, being similar to an ideal simple metal. The rapid decay of ϵ'' expresses viscous electron damping due to scattering processes associated with the electrical resistivity. The real part of the dielectric function is negative and diverges for $\omega \rightarrow 0^{+}$, in agreement with the formation of a free electron gas upon Al doping. Notably, because the wave functions for a a free-electron gas are fairly uniformly distributed throughout the material, the field acting on electrons is just an average field. This, along with the agreement with the experimental results,[53] confirms *a posteriori* the validity of the Drude−Lorentz model for this compound without any need for local-field corrections and/or many-body corrections beyond the mean field level for this energy range.

Where $\epsilon' = 0$ and $\epsilon'' \ll 1$, the loss function (blue line, Figure 2) has a peak, corresponding to the plasma frequency (ω_p) of the system. The presence of Al dopants imparts a drastic shift of the plasma frequency (see Figure 2), that moves from the far-UV (~17 eV,[54] not shown) in the case of ZnO to the near-IR (NIR) and visible range in the case of AZO, in agreement with recent experimental results.[25,35−37] It is relevant to note that, while the plasma frequency for noble metals is an intrinsic property of the material that cannot be changed, in the case of TCOs, ω_p can be tuned by controlling the electron density, i.e., by changing the doping. This is evident from Figure 2 and Table 1, which summarizes the plasma frequency values

Table 1. Plasma Frequencies (Wavelengths) ω_p (λ_p) and Free Charge Concentration N_e of AZO Bulk; SPP Frequencies (Wavelengths) ω_{SPP} (λ_{SPP}) of AZO/ZnO Interfaces, at Different Al Concentrations (0.8, 1.6, and 3.2%)

	ω_p (λ_p)	N_e (cm^{-3})	ω_{SPP} (λ_{SPP})
0.8%	0.95 eV (1.31 μm)	1.9×10^{20}	0.48 eV (2.58 μm)
1.6%	1.71 eV (0.73 μm)	6.1×10^{20}	0.86 eV (1.44 μm)
3.2%	2.03 eV (0.61 μm)	8.7×10^{20}	1.02 eV (1.21 μm)

obtained for AZO at different Al percentages. Increasing doping, the plasmonic peak in EELS moves at higher energies and splits due to the resulting anisotropic Al distribution, which is responsible for a dis-homogeneous Al−Al and Al−O interaction along the three spatial directions in the supercell. Even in the heavy doping regime (e.g., 3.2%), the plasma frequency does not overlap with the interband transition energy region (E > 3.5 eV). This assures low losses in the NIR-vis range, reducing one of the most challenging problems that plagues standard metallic materials. For instance, the optical losses in AZO films have been measured to be ~5 times smaller than Ag films in the NIR.[25]

The tunability of the plasma frequency has remarkable applicative repercussions: (i) it allows one to handle the frequency operating region of the TCOs as intrinsic plasmonic materials in connection with other dielectric layers for realization of metamaterials and SPP waveguides; (ii) it can be exploited in combination with metal plasmonic systems as epsilon-near zero (ENZ) materials. In the latter case, the (frequency dependent) reduction of the permittivity of the TCO, below that of a vacuum, is used to modify the surface plasmon polariton characteristics of the metallic part.[29]

Inverting eq 2, we can estimate the free electron concentration N_e available in the conduction band. The results (see Table 1) are of the order of 10^{20} cm^{-3}. Similar results would be obtained evaluating the injected charge density from

dx.doi.org/10.1021/ph500118y | ACS Photonics 2014, 1, 703−709

the expression for the free electron gas, $N_e = k_F^3/(3\pi^2)$, where k_F is the Fermi wavenumber. The relation between doping ratio and free charge is not linear: reaching the solubility limit, the free charge donated by Al is decreased because of the establishment of Al−Al and Al−O clustering interactions,[31] which tend to localize the electron charge. This is responsible for the splitting of the plasma peak in EELS spectra, discussed above (Figure 2).

$N_e \sim 10^{20}$ cm^{-3} is a remarkable carrier concentration for standard doped semiconductors, (e.g., Si, GaAS)[55] and well beyond the practical minimum threshold (10^{19} cm^{-3}), necessary for sustaining collective electronic oscillations (plasmons) in bulk systems. Our carrier density results are in agreement with most experimental data ($N_e \sim 10^{20}$ cm^{-3}); however, they do not cover the large variability range ($N_e \in [10^{19}-10^{21}]$ cm^{-3}), collected among the experimental reports.[30,35−37] We note, however, that (i) the experimental results are often obtained at very different doping levels (up to 7.5%[56]) and (ii) our simulations refer to ideal semiconducting ZnO crystals and not to almost n-degenerate samples, as in typical experimental cases. Furthermore, the simultaneous presence of intrinsic impurities (e.g., H) or defects (e.g., oxygen vacancy) may affect the free electron density, as recently demonstrated.[10,25]

SURFACE-PLASMON POLARITON AT THE AZO/ZNO INTERFACE

To fully describe the potential of ZnO-based systems for plasmonic applications, we finally considered the electronic properties of the AZO/ZnO interface, which actually behaves as a metal/dielectric interface that can sustain SPP formation and propagation. The fundamental properties of a SPP excitation at the interface between two semi-infinite planar layers of AZO and ZnO were investigated as a function of Al doping. By exploiting classical electromagnetism arguments, the frequency of the SPP mode can be defined as $\omega_{SPP} = \omega_p/(1 + \epsilon_d^\infty)^{1/2}$. Since for ZnO $\epsilon^\infty = 3$, the AZO plasma frequency is halved as a result of the formation of the AZO/ZnO interface (see Table 1).

SPPs are characterized in terms of their dispersion relations and characteristic lengths. The dispersion relation gives the relationship between the frequency (ω) and the wavevector ($\hat{k}_{SPP}$) of the excitation in the plane along which it propagates. $\hat{k}_{SPP}(\omega) = k'_{SPP}(\omega) + ik''_{SPP}(\omega)$ is a complex quantity, whose real part (k') determines the SPP wavelength, while the imaginary part (k'') accounts for the damping of the SPP along the interface. The real and imaginary parts of $\hat{k}_{SPP}$ can be expressed as

$$k'_{SPP}(\omega) = k_0\left(\frac{\epsilon'_d(\omega)\epsilon'_m(\omega)}{\epsilon'_d(\omega) + \epsilon'_m(\omega)}\right)^{1/2} \quad (3)$$

$$k''_{SPP}(\omega) = k_0\frac{\epsilon''_m(\omega)}{2[\epsilon'_m(\omega)]^2}\left(\frac{\epsilon'_d(\omega)\epsilon'_m(\omega)}{\epsilon'_d(\omega) + \epsilon'_m(\omega)}\right)^{3/2} \quad (4)$$

where $k_0 = 2\pi/\lambda_0$ is the light wavevector in the free space; ϵ'_d and ϵ'_m (ϵ''_m) are the real (imaginary) part of the frequency-dependent dielectric function of the dielectric and metal systems, respectively. In the dielectric medium, the dispersion radiation of light is a straight line, with slope $(\epsilon_d^\infty)^{1/2}$.

By assuming ZnO as the dielectric and AZO as the metal and inserting the results of Figure 2 into eq 3, we can obtain the dispersion relations for the AZO/ZnO interface at different Al concentrations. The complete dispersion relation would exhibit a divergence for $\omega = \omega_p$, giving rise to high and low energy branches: only the low energy branch is displayed in Figure 3.

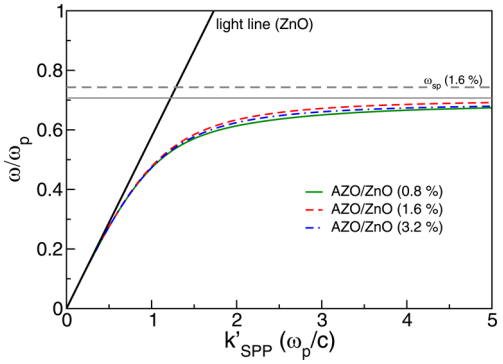

Figure 3. Dispersion relation of the real part of the SPP wavevector k'_{SPP} of AZO/ZnO interfaces at different Al concentrations. The thick black line marks the dispersion relation for light in the ZnO region. Horizontal solid and dashed gray lines define the asymptotic AZO surface plasmon frequency, i.e., for the AZO/air interface, at 1.6% Al content. The solid line corresponds to the ideal interface (i.e., $\omega = \omega_p/(2)^{1/2}$), while the dashed line is obtained from explicit surface slab calculation.

The high energy branch (Brewster mode) does not describe a surface wave. This corresponds to the fact that for $\omega > \omega_p$ the metal is no more reflecting, becoming transparent to the incoming radiation (no plasmons are excited). At low frequencies, the surface mode asymptotically approaches the light line for ZnO (black line). As the frequency increases, the SPP mode separates from the light line and approaches the surface plasmon frequency (ω_{sp}) of the conductor (AZO). Figure 3 shows the asymptotic surface plasmon frequency (i.e., AZO/air interface) for AZO at 1.6% Al doping, obtained in two different ways. In one case (solid thin line), $\omega_{sp} = \omega_p/(2)^{1/2}$ derives from the combination of the bulk dielctric constant of AZO and air. In the second case (dashed line), ω_{sp} is directly calculated from a slab simulation. The two values are very similar and confirm the validity of the present approach. The fact that k'_{SPP} is always larger than the corresponding light line is indicative of the nonradiative nature of the SPP mode. The different Al doping does not significatively change the dispersion relation (see Figure 3).

From the complex $\hat{k}_{SPP}(\omega)$, we can derive the length scales that characterize the spatial profile of the SPP mode for the AZO/ZnO ideal interface as a function of the incoming radiation (λ_0) and of Al doping, as shown in Figure 4. For the potential application of these materials in telecommunication devices, we mark the corresponding characteristic wavelength (1.5 μm) with a vertical line. It is evident from Figure 4 that doping, namely, the free electron density, affects the threshold of those characteristic lengths, which amounts to ∼0.9−1.1 μm for 1.6−3.2% Al content and ∼1.9 μm for 0.8% dosage. Thus, AZO can support SPPs at the telecom wavelengths for medium-high doping levels (1.6−3.2%), while SPPs are not active for lower doping.

The SPP profile can be described in terms of wavelength (λ_{SPP}), propagation length (δ_{SPP}), and dielectric (δ_d) and metal (δ_m) penetration depths.

dx.doi.org/10.1021/ph500118y | ACS Photonics 2014, 1, 703−709

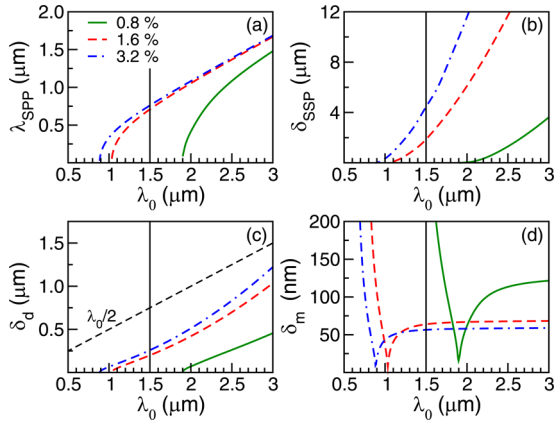

Figure 4. Characteristic lengths of SPP in AZO/ZnO interfaces at different Al concentrations. Vertical black lines mark the characteristic wavelength for telecommunications. The dashed line in panel c corresponds to the upper compactness limit $\delta_d = \lambda_0/2$.

The SPP wavelength (λ_{SPP}) is obtained from the real part of the wavevector

$$\lambda_{SPP} = \frac{2\pi}{k'_{SPP}} = \lambda_0 \sqrt{\frac{\epsilon'_d + \epsilon'_m}{\epsilon'_d \epsilon'_m}} \tag{5}$$

and defines the period of the wave associated with the SPP oscillation. In the case of the AZO/ZnO interface, λ_{SPP} (panel a) is of the order of ∼1.0 μm. Since λ_{SPP} defines the periodicity of the SPP wave, it also defines the scale of optical structures (e.g., Bragg scatterers) typically used to control the SPP.

The propagation length (δ_{SPP}) is defined as the distance over which the intensity of the SPP mode falls to $1/e$ of its initial value and derives from the imaginary part of $\hat{k}_{SPP}(\omega)$ through the relation

$$\delta_{SPP} = \frac{1}{2k''_{SPP}} = \lambda_0 \frac{(\epsilon'_m)^2}{2\pi\epsilon''_m} \left(\frac{\epsilon'_d + \epsilon'_m}{\epsilon'_d \epsilon'_m} \right)^{3/2} \tag{6}$$

In most systems, $|\epsilon'_m| \gg |\epsilon'_d|$ and eq 6 reduces to $\delta_{SPP} \propto (\epsilon'_m)^2/\epsilon''_m$. Thus, long propagation lengths are obtained with plasmonic materials that exhibit large negative ϵ' (i.e., high conductivity) and small ϵ'' (i.e., low energy loss), characteristics fulfilled by AZO. For any real application, it is necessary that $\delta_{SPP} > \lambda_{SPP}$; i.e., SPP should propagate as a straight ray in geometrical optics. This seems to be the case also for the AZO/ZnO interface, where the SPP can propagate up to a few microns also at the telecom wavelength (Figure 4, panel b). These values are still 2 orders of magnitude smaller than the maximum propagation lengths obtained with Ag plasmonic components.[11] However, the study of TCOs as plasmonic materials is at its infancy; thus, the optimization of the surface geometries and of the loss processes might easily improve the performances of this class of materials.

The penetration lengths into the dielectric and metallic layers are defined as

$$\delta_d = \frac{\lambda_0}{2\pi} \left| \frac{\epsilon'_d + \epsilon'_m}{(\epsilon'_d)^2} \right|^{1/2} \tag{7}$$

$$\delta_m = \frac{\lambda_0}{2\pi} \left| \frac{\epsilon'_d + \epsilon'_m}{(\epsilon'_m)^2} \right|^{1/2} \tag{8}$$

and determine the compactness of the SPP, giving a measure of the minimum thickness required for the dielectric and metal layers. The need for high localization at interfaces imposes the penetration depths to be as small as possible. This is realized for high values of the real part of the dielectric function, which dominates the denominators of eqs 8. In the case of δ_d, a high ϵ'_d corresponds to a high refractive index of the dielectric layer, while, in the case of δ_m, it corresponds to high conductivity.

The penetration length inside the ZnO layer δ_d (panel c) is very short (∼200 nm depending on Al content) at $\lambda = 1.5$ μm, giving rise to a high compact optical system. In order to highlight this feature, we reported (black dashed line, panel c) the so-called *upper compactness limit* $\delta_d = \lambda_0/2$, which corresponds to the minimal diameter spot of a dielectric photonic device. The fact that for the AZO/ZnO interface δ_d is always below the $\lambda_0/2$ line[56] indicates that the SPP mode has the electromagnetic field enhancement properties typical of photonic systems and the subwavelength confinement of electronic devices. Recently, short decay lengths have been predicted for other TCOs (such as ITO).[57] Notably, standard plasmonic materials such as Au and Ag do not fulfill this requirement, crossing the compactness limit in the range 300–500 nm.[26]

The skin-depth properties of the metallic layer are quantified in terms of the penetration length inside the metal δ_m (panel d). In the present case, δ_m is at least 2 orders of magnitude smaller than the corresponding δ_d for each considered doping. At low wavelengths, corresponding to $\omega > \omega_p$, the metal layer is no more reflecting and becomes transparent to the incoming radiation, i.e., the δ_m diverges, while, for higher wavelengths, δ_m rapidly reaches a plateau.

As a final analysis of the AZO/ZnO planar interface, we evaluated the figure of merit (Q) for the SPP mode and for transformation optics (TO), which are defined as[58]

$$Q_{SPP} = \frac{k'_{SPP}(\omega)}{k''_{SPP}(\omega)} = \frac{\epsilon'_d + \epsilon'_m}{\epsilon'_d \epsilon'_m} \frac{(\epsilon'_m)^2}{\epsilon''_m} \tag{9}$$

$$Q_{TO} = \frac{1}{\epsilon''_m} \tag{10}$$

The results are summarized in Figure 5. In the case of SPP (panel a), the figure of merit represents the ratio between the confinement (k'_{SPP}) and the attenuation (k''_{SPP}) measure. Q_{SPP} is particularly sensitive to the doping level, with the value for 3.2% Al content being almost double that for 1.6% dosage. In the case of transformation optics, the figure of merit is mainly dictated by the imaginary part of the metal dielectric function,

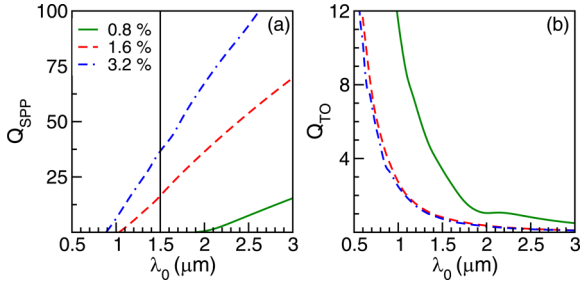

Figure 5. Figure of merit for (a) surface plasmon polariton and (b) transformation optics. Vertical black lines mark the characteristic wavelength for telecommunications.

dx.doi.org/10.1021/ph500118y | ACS Photonics 2014, 1, 703–709

and thus directly associated with interband dissipation processes. Since the optical absorption edge of AZO is in the UV, i.e., low loss in the NIR-vis range, Q_{TO} is higher than the corresponding value for Au and Ag metals, confirming that doped ZnO is a realistic choice also for TO devices in the NIR and telecom wavelengths.[30]

CONCLUSION

We present a first-principles investigation of the plasmonic properties of Al-doped ZnO as a function of the Al contents. Our results indicate that AZO acts as a TCO, coupling transparency in the visible range and metal-like conductivity for a large range of metal doping. The intrinsic electronic properties of the ZnO host facilitate the formation of a free electron gas upon doping, which can be excited in the near-IR/visible range to give plasma oscillations. The plasma frequency and the complex dielectric function of AZO may be easily tailored controlling the doping level and/or the presence of defects and impurities.

We furthermore characterize the SPP properties of a planar AZO/ZnO interface, that have been recently proposed for metamaterials and telecom applications. The good agreement with the experimental results confirms also the validity of the Drude−Lorentz model in the description of this class of materials that present a unique and well dispersive conduction band bottom. Indeed, nonparabolic deviations of the conduction band, which have been invoked to describe renormalization effects on the optical gap and on the onset of the optical transitions of doped ZnO in the UV range,[47,59,60] have instead negligible effects in the plasmon active energy range (i.e., NIR-vis).

The combination of a plasmonic activity in the NIR-vis and the low energy loss, along with the long SPP wavelength ($\simeq$1 μm) and short decay lengths ($\simeq$200 nm) that we predict, make AZO a promising and cheap plasmonic material, alternative to standard noble metals (e.g., Au, Ag), for a wide range of applications from sensing to optolectronic devices and telecommunications.

ASSOCIATED CONTENT

Supporting Information

Details on the Drude−Lorentz approach adopted in the present work. This material is available free of charge via the Internet at http://pubs.acs.org.

AUTHOR INFORMATION

Corresponding Author

*E-mail: arrigo.calzolari@nano.cnr.it.

Notes

The authors declare no competing financial interest.

ACKNOWLEDGMENTS

We acknowledge support from University of Modena and Reggio Emilia, through grant 'Nano- and emerging materials and systems for sustainable technologies' and funding from the European Union Seventh Framework Programme under grant agreement no. 265073 (ITN-Nanowiring). Computational resources were provided at CINECA through project IscraC_DopOX.

REFERENCES

(1) Tame, M.; McEnery, K.; Özdemir, S. K.; Lee, J.; Maier, S.; Kim, M. Quantum plasmonics. *Nat. Phys.* **2013**, *3*, 329−340.
(2) Berweger, S.; Atkin, J. M.; Olmon, R. L.; Raschke, M. B. Light on the tip of a needle: plasmonic nanofocusing for spectrometry on the nanoscale. *J. Phys. Clem. Lett.* **2012**, *3*, 945−952.
(3) Hess, O.; Pendry, J. B.; Maier, S. A.; Oulton, R. F.; Hamm, J. M.; Tsakmakidis, K. L. Active nanoplasmonic metamaterials. *Nat. Mater.* **2012**, *11*, 573−584.
(4) Kildishev, A. V.; Boltasseva, A.; Shalev, V. M. Planar photonics with metasurfaces. *Science* **2013**, *339*, 1232009 (1−6).
(5) Abb, M.; Sepulveda, B.; Chong, H. M. H.; Muskens, O. L. Transparent conductive oxides for active hybrid metamaterials. *J. Opt.* **2012**, *14*, 114007 (1−7).
(6) Gao, S.; Ueno, K.; Misawa, H. Plasmonic antenna effects on photochemical reactions. *Acc. Chem. Res.* **2011**, *44*, 251−260.
(7) Cubukcu, E.; Kort, E. A.; Crozier, B.; Capasso, F. Plasmonic laser antenna. *Appl. Phys. Lett.* **2006**, *89*, 093120 (1−3).
(8) Guo, X.; Qiu, M.; Bao, J.; Wiley, B.; Yang, Q.; Zhang, X.; Ma, Y.; Yu, H.; Tong, L. Direct coupling of plasmonic and photonic nanowires for hybrid nanophotonic component and circuits. *Nano Lett.* **2009**, *9*, 4515−4519.
(9) Lawrie, B.; Kim, K.-W.; Norton, D.; Haglund, R., Jr. Plasmon-exciton hybridization in ZnO quantum well al nanodisc hetros-tructures. *Nano Lett.* **2012**, *12*, 6152−6157.
(10) Sachet, E.; Losego, M.; Guske, J.; Franzen, S.; Maria, J.-P. Mid-infrared surface plasmon resonance in zinc oxide semiconductor thin films. *Appl. Phys. Lett.* **2013**, *102*, 051111 (1−3).
(11) Dionne, J.; Sweatloch, L.; Atwater, H.; Polman, A. Planar metal plasmon waveguides: frequency-dependent dispersion, propagation, localization and loss beyond the free electron model. *Phys. Rev. B* **2005**, *72*, 075405 (1−11).
(12) Atwater, H.; Polmann, A. Plasmonics for improved photovoltaic devices. *Nat. Mater.* **2010**, *9*, 205−213.
(13) Thomann, I.; Pinaud, B. A.; Chen, Z.; Clemens, B. M.; Jaramillo, T. F.; Brongersma, M. L. Plasmon Enhanced Solar-to-Fuel Energy Conversion. *Nano Lett.* **2011**, *11*, 3440−3446.
(14) Zhao, X.; Wang, P.; Li, B. Surface plasmon enhanced energy transfer in metal-semiconductor hybrid nanostructures. *Nanoscale* **2011**, *3*, 3056−3059.
(15) Pradhan, A.; Holloway, T.; Mundle, R.; Dondapali, H.; Bahoura, M. Energy harvesting in semiconductor-insulator-semiconductor junctions through excitation of surface plasmon polariton. *Appl. Phys. Lett.* **2012**, *100*, 061127 (1−3).
(16) Lin, Y.-G.; Hsu, Y.-K.; Chen, Y.-C.; Wang, S.-B.; Miller, J.; Chen, L.-C.; Chen, K.-H. Plasmonic Ag/Ag3(PO4)1-x nanoparticle photo-sensitized ZnO nanorod-array photoanodes for water oxidation. *Energy Environ. Sci.* **2012**, *5*, 8917−8922.
(17) Kneipp, K.; Kneipp, H.; Itzkan, I.; Dasari, R. R.; Feld, M. S. Ultrasensitive Chemical Analysis by Raman Spectroscopy. *Chem. Rev.* **1999**, *99*, 2957−2976.
(18) Morton, S. M.; Silverstein, D. W.; Jensen, L. Theoretical studies of plasmonics using electronic structure Methods. *Chem. Rev.* **2011**, *111*, 3962−3994.
(19) Haes, A. J.; Hall, W. P.; Chang, L.; Klein, W. L.; Duyne, R. P. V. A Localized Surface Plasmon Resonance Biosensor: First Steps toward an Assay for Alzheimer's Disease. *Nano Lett.* **2004**, *4*, 1029−1034.
(20) Prokes, S.; Glembocki, O.; Rendell, R.; Ancona, M. Enhanced plasmon coupling in crossed dielectric-metal nanowire composite geometries and applications to surface enhanced Raman spectroscopy. *Appl. Phys. Lett.* **2007**, *90*, 093105(1−3).
(21) Shen, H.; Shan, C.-X.; Qiao, Q.; Liu, J.-S.; Li, B.-H.; Shen, D.-Z. Stable surface plasmon enhanced ZnO homojunction light emitting devices. *J. Mater. Chem. C* **2013**, *1*, 234−237.
(22) Qiao, Q.; Shan, C.-X.; Zheng, J.; Li, B.-H.; Zhang, Z.-Z.; Zhang, L.-G.; Shen, D.-Z. Localized surface plasmon enhanced light-emitting devices. *J. Mater. Chem.* **2012**, *22*, 9481−9484.
(23) Tang, W.; Huang, D.; Wu, L.; Zhao, C.; Xu, L.; Gao, H.; Zhang, X.; Wang, W. Surface plasmon enhanced ultraviolet emission and

observation of random lasing from self-assembly Zn/ZnO composite nanowires. *CrystEngComm* **2011**, *13*, 2336−2339.
(24) Zhang, Y.; He, X.; Li, J.; Li, K.; Yue, C.; Wu, Z.; Wu, S.; Kang, J. Band edge emission enhancement by quadrupole surface plasmon exciton coupling using direct contact Ag/ZnO nanospherets. *Nanoscale* **2013**, *5*, 574−580.
(25) Kim, H.; Prokes, M. O.; Glembocki, S. M.; Piqué, O. J. A. Optimization of Al-doped ZnO films for low loss plasmonic materials at telecommunication wavelengths. *Appl. Phys. Lett.* **2013**, *102*, 171103 (1−3).
(26) Noginov, M. A.; Gu, L.; Livenere, J.; Zhu, G.; Pradhan, A. K.; Mundle, R.; Bahoura, M.; Barnakov, Y. A.; Podolskiy, V. A. Transparent conductive oxides: Plasmonic materials for telecom wavelengths. *Appl. Phys. Lett.* **2011**, *99*, 021101 (1−3).
(27) Wooten, F. *Optical Properties of Solids*; Academic Press, Inc.: San Diego, CA, 1972.
(28) Ellmer, K. Past achievements and future challanges in the development of optically transparent electrodes. *Nat. Photonics* **2012**, *6*, 809−817.
(29) Traviss, D.; Bruck, R.; Mills, B.; Abb, M.; Muskens, O. L. Ultrafast plasmonics using transparent conductive oxide hybrids in the epsilon-near-zero regime. *Appl. Phys. Lett.* **2013**, *102*, 121112 (1−4).
(30) Naik, G. V.; Shalaev, V. M.; Boltasseva, A. Alternative Plasmonic Materials: beyond gold and silver. *Adv. Mater.* **2013**, *25*, 3264−3294.
(31) Bazzani, M.; Neroni, A.; Calzolari, A.; Catellani, A. Optoelectronic properties of Al:ZnO: Critical dosage for an optimal transparent conductive oxide. *Appl. Phys. Lett.* **2011**, *98*, 121907 (1−3).
(32) Gabás, M.; Piero, M.; Barrett, P.; Sacchio, N. T.; Bruneval, M.; Cui, F.; Simonelli, Y.; Diaz-Carrasco, L.; Ramos Barrado, P. J. R. Direct observation of Al-doping-induced electronic states in the valence band and band gap of ZnO films. *Phys. Rev. B* **2011**, *84*, 153303 (1−4).
(33) Brillson, L. J.; Lu, Y. ZnO Schottky barriers and Ohmic contacts. *J. Appl. Phys.* **2011**, *109*, 121301(1−33).
(34) Catellani, A.; Calzolari, A.; Ruini, A. Effect of ultrathin gold on the Ohmic-to-Schottky transition in Al/ZnO contacts: A first-principles investigation. *J. Appl. Phys.* **2014**, *115*, 043711 (1−4).
(35) Noh, J. H.; Jung, H. S.; Lee, J.-K.; Kim, J. Y.; Cho, C. M. sul An, J.; Hong, K. S. Reversible change in electrical and optical properties in epitaxially grown Al-doped ZnO thin films. *J. Appl. Phys.* **2008**, *104*, 073706 (1−5).
(36) Frölich, A.; Wegener, M. Spectroscopic characterization of highly doped ZnO films grown by atomic-layer deposition for three dimensional infrared metamaterials. *Opt. Mater. Express* **2011**, *1*, 883−889.
(37) Naik, G. V.; Liu, J.; Kildishev, A.; Shalaev, V. M.; Boltasseva, A. Demonstration of Al:ZnO as plasmonic component for near infrared metamaterials. *Proc. Natl. Acad. Sci. U. S. A.* **2012**, *109*, 8834−8838.
(38) Colle, R.; Parruccini, P.; Benassi, A.; Cavazzoni, C. Optical properties of emeraldine salt polymers from ab initio calculations: comparison with recent experimental data. *J. Phys. Chem. B* **2007**, *111*, 2800−2805.
(39) Perdew, J. P.; Burke, K.; Ernzerhof, M. Generalized Gradient Approximation Made Simple. *Phys. Rev. Lett.* **1996**, *77*, 3865−3868.
(40) Vanderbilt, D. Soft self-consistent pseudopotentials in a generalized eigenvalue formalism. *Phys. Rev. B* **1990**, *41*, R7892−R7895.
(41) Calzolari, A.; Ruini, A.; Catellani, A. Anchor group versus conjugation: towards the gap-state engineering of functionalized ZnO(10−10) surface for optoelectronic applications. *J. Am. Chem. Soc.* **2011**, *133*, 5893−5899.
(42) Janotti, A.; Segev, D.; Van de Walle, C. G. Effects of cation *d* states on the structural and electronic properties of III-nitride and II-oxide wide-band-gap semiconductors. *Phys. Rev. B* **2006**, *74*, 045202 (1−9).
(43) Dong, Y.; Brillson, L. First-Principles Studies of Metal (111)/ZnO0001 Interfaces. *J. Electron. Mater.* **2008**, *37*, 743−748.
(44) Young, D. L.; Coutts, T. J.; Kaydanov, V. I.; Gilmore, A. S.; Mulligan, W. P. Direct measurement of density-of-states effective mass and scattering parameter in transparent conducting oxides using second-order transport phenomena. *J. Vac. Sci. Technol., A* **2000**, *18*, 2978−2985.
(45) Mondragon-Suarez, H.; Maldonado, A.; de la L Olvera, M.; Reyes, A.; Castanedo-Perezc, R.; Torres-Delgado, G.; Asomoza, R. ZnO:Al thin films obtained by chemical spray: effect of the Al concentration. *Appl. Surf. Sci.* **2002**, *193*, 52−59.
(46) Formally, clean ZnO presents a unique and well dispersive sp conduction band bottom, that can be described by a quasi-parabolic effective mass, averaged in the three directions. Nonparabolic contributions which become increasingly relevant at increasing doping levels have been observed.[47] We wish to point out however that our results should not be affected by a more accurate description of the optical gap and onset of optical transitions, with the energy range of application described here being completely different.
(47) Schleife, A.; Rödl, C.; Fuchs, F.; Furthmüller, J.; Bechstedt, F. Optical and energy-loss spectra of MgO, ZnO, and CdO from ab initio many-body calculations. *Phys. Rev. B* **2009**, *80*, 035112 (1−10).
(48) Ashkenov, N.; Mbenkum, B.; Bundesmann, C.; Riede, V.; Lorenz, M.; Spemann, S.; Wagner, G.; Neumann, H.; darakchieva, V.; Arwin, H.; Monemar, B. Infrared dielectric functions and phonon modes of high quality ZnO films. *J. Appl. Phys.* **2003**, *93*, 126−133.
(49) Noel, Y.; Zicovich-Wilson, C. M.; Civalleri, B.; D'Arco, P.; Dovesi, R. Polarization properties of ZnO and BeO: An ab initio study through the Berry phase and Wannier functions approaches. *Phys. Rev. B* **2002**, *65*, 014111.
(50) Calzolari, A.; Buongiorno Nardelli, M. Dielectric properties and Raman spectra of ZnO from a first principles finite-differences/finite-fields approach. *Sci. Rep.* **2013**, *3*, 2999 (1−6).
(51) The well-known ZnO emissions in the visible range (e.g., green-band emission) are mostly originated by point defects, such as Zn vacancy. The presence of these features does not change the present analysis and goes beyond the aim of this work.
(52) Moss, T. S. The Interpretation of the Properties of Indium Antimonide. *Proc. Phys. Soc.* **1954**, *67*, 775.
(53) Fujiwara, H.; Kondo, M. Effects of carriers concentration on the dielectric function of ZnO:Ga and In2O3:Sn studied by spectroscopic ellipsometry: analysis of free carrier and band edge adsorption. *Phys. Rev. B* **2005**, *71*, 075109 (1−10).
(54) Huang, M. R. S.; Erni, R.; Lin, H.-Y.; Wang, R.-C.; Liu, C.-P. Characterization of wurtzite ZnO using valence electron energy loss spectroscopy. *Phys. Rev. B* **2011**, *84*, 155203 (1−6).
(55) Hoffman, A. J.; Alekseyev, L.; Howard, S. S.; Franz, K. J.; Wasserman, D.; Podolskiy, V. A.; Narimanov, E. E.; Sivco, D. L.; Gmachl, C. Negative refraction in semiconductor metamaterials. *Nat. Mater.* **2007**, *6*, 946−950.
(56) Badalawa, W.; Matsui, H.; Ikehata, A.; Tabata, H. Surface plasmon modes guided by Ga-doped ZnO layers bounded by different dielectrics. *Appl. Phys. Lett.* **2011**, *99*, 011913 (1−3).
(57) Abb, M.; Wang, Y.; Papasimakis, N.; de Groot, C. H.; Muskens, O. L. Surface-Enhanced Infrared Spectroscopy Using Metal Oxide Plasmonic Antenna Arrays. *Nano Lett.* **2014**, *14*, 346−352.
(58) Berini, P. Figure of merit for surface plasmon waveguide. *Opt. Express* **2007**, *14*, 13030−13042.
(59) Kim, J. S.; Jeong, J.-H.; Park, J. K.; Baik, Y. J.; Kim, I. H.; Seong, T.-Y.; Kim, W. M. Optical analysis of doped ZnO thin films using non-parabolic conduction-band parametrers. *J. Appl. Phys.* **2012**, *111*, 123507 (1−9).
(60) Tang, K.; Gu, S.; Ye, J.; Huang, S.; Gu, R.; Zhu, S.; Zhang, R. Temperature-dependent exciton-related transitions energies mediated by carrier concentrations in unintentional Al-doped ZnO films. *Appl. Phys. Lett.* **2013**, *102*, 221905 (1−5).